Effects of Catalytic Boundary Conditions Accounting for Incomplete Chemical Energy Accomodation

M. Barbato* V. Bellucci†
CRS4 Research Centre – Cagliari, Italy

and

C. Bruno‡
Università di Roma I – Roma, Italy

Abstract

The Chemical Energy Accomodation process occurring to gas atoms recombining catalytically on a solid surface is briefly presented. Due to the relevance this phenomenon might have for Thermal Protection Systems heat loads, an analysis of experimental data and recent models accounting for it is done.

Information on the Chemical Energy Accomodation Coefficient β available so far from simple Langmuir-Hinshelwood or Eley-Rideal models is still not sufficient to draw final conclusions in regard to its behaviour with temperature and pressure, even for pure metals and SiO_2. Using a hypersonic flow solver, a parametric analysis of the effect of varying β is presented for nickel coated bodies past hypersonic air flows; catalytic boundary conditions have been modified to account for incomplete chemical energy accomodation. Effects on body heat load, gas temperature and degree of dissociation are examined. Large effects have been found for thermal loads whereas modest were the effects on gas composition.

*Research Engineer, CRS4 Research Centre, Via Nazario Sauro 10, Cagliari 09123, Italy.

†Research Engineer, CRS4 Research Centre, Via Nazario Sauro 10, Cagliari 09123, Italy.

‡Associate Professor, Dipartimento di Meccanica e Aeronautica, Università di Roma I, Via Eudossiana 18, Roma 00184, Member AIAA.

Nomenclature

c_p	specific heat at constant pressure, J/kg K
D	dissociation energy, J/mole
$\mathcal{D}_s$	multi-diffusion coefficient, m^2/s
e	total energy per unit mass J/kg
e_V	vibrational-electronic energy per unit mass J/kg
h	enthalpy, J/kg
h^0	formation enthalpy, J/kg
k_{tr}	thermal conductivity for translational and rotational energy, J/m s
k_V	thermal conductivity for vibrational and electronic energy, J/m s
L	body main dimension, m
Ma	Mach number
n	coordinate perpendicular to the body surface, m
p	pressure, Pa
Q	energy, J/mole
$\dot{q}$	heat flux, W/m^2
T	temperature, K
$\mathbf{u}$	velocity vector
X_s	molar fraction of s chemical species
Y_s	mass fraction of s chemical species
β	chemical energy accomodation factor
ϵ	surface emissivity factor
γ	energy-transfer catalytic recombination coefficient
γ'	atomic recombination coefficient
μ	mixture viscosity
θ	surface coverage: ratio between # of occupied and total # of available sites on the catalyst surface
ρ	mass density, kg/m^3
σ	Stefan-Boltzmann constant W/ m^2 K^4

Subscripts

ads	adsorption
g	gas
R	radiative

rec	recombined
s	chemical species index
tr	translational-rotational
V	vibrational-electronic
w	wall
∞	free stream condition

Superscript

$*$	adsorbed atom
r	rotational
t	translational

Introduction

The effort spent by the aerospace research community to understand and model catalytic recombination of atomic species at solid walls such as thermal protection surfaces of re-entry space vehicles and future space-planes is shown by the number of models set up in the past years [1], [2].

When dealing with these phenomena one of the main processes to face is Chemical Energy Accomodation (CEA), i.e., release of chemical energy to the catalyst surface done by catalytically formed molecules. The importance of CEA has been underlined by many authors on the basis of experimental finding [3, 4, 5, 6] and the effects of the consequent production of excited molecules from a catalytic surface may have for gas-wall heat exchange and near wall gas chemistry have been also investigated [7, 8].

Some of the heterogeneous catalysis models found in the literature [9, 10, 11, 12], define recombination coefficients assuming full CEA, i.e., the atomic recombination coefficient γ' coincides with the energy-transfer catalytic recombination coefficient γ. This approximation is usually used due to the complexity of the energy accomodation process and to the associated scant knowledge of reliable quantitative informations for technical surfaces such as those of Thermal Protection Systems (TPS).

Some more recent models for heterogeneous catalysis on TPS surfaces have included the effects of partial chemical energy accomodation for recombined molecules. The Suslov and Tirskiy model [13], for instance, accounts for incomplete accomodation of N_2 molecules when formed catalytically via the Eley-Rideal (ER) mechanism (see Table 1) on Reaction Cured Glass surfaces. Their model for the process of energy accomodation takes into account wall quenching of excited molecules also. Therefore the coefficient β found in [13] accounts for non complete CEA and wall quenching, and, calculated at several pressures ($10^{-4} \div 1$ atm), varies from 0.3 to 1 when T_w varies from 1000 to 2000 K.

The model of Daiß et al. [14] accounts for both ER and Langmuir-Hinshelwood (LH) recombination mechanisms (see Table 1) and for dissociative adsorption too. LH-formed molecules are assumed fully accommodated, whereas for ER-formed N_2 and O_2 β ($\neq 1$) is modeled. These authors have found β_{O_2} decreasing from 0.34 to 0.3 when T goes from 300 to 2000 K, and β_{N_2} decreasing from 0.62 to 0.53 in the same temperature range.

Even though, Suslov and Tirskiy have accounted for wall quenching of excited molecules and Daiß et al. have not, the disagreement between the two trends for β_{N_2} needs to be resolved. This shows the uncertainties still existing in understanding and modeling the CEA process. In the following a discussion on the Chemical Energy Accomodation mechanism will be presented. Furthermore, a simple way to account for $\beta \neq 1$ in a thermochemical non-equilibrium CFD code is proposed and the results obtained are discussed.

Chemical Energy Accomodation

Chemical energy accomodation can be described taking as an example the ER mechanism of catalytic recombination. The first elementary step to consider is the adsorption of a single atom:

$$A + * \rightarrow A^*$$

where $*$ represents an adsorption surface site and A^* is a chemisorbed atom, i.e. an atom chemically bonded to the catalyst. We assume that all the adsorption energy, Q_{ads}, is deposited on the catalyst. The elementary step representing the Eley-Rideal recombination mechanism is:

$$A + A^* \rightarrow A_2 + *$$

where we assume that after recombination the A_2 molecule leaves the surface. This reaction is exothermic and the energy release (per mole) is:

$$Q_{rec} = D - Q_{ads}$$

where D is the A_2 bond energy. Depending on the residence time, the recombined molecule can leave this energy in part or totally on the catalyst surface. Two limit situations can be foreseen:

full accomodation when Q_{rec} is totally released to the catalyst:

$$Q_{cat} = Q_{ads} + (D - Q_{ads}) \equiv D$$

no accomodation when Q_{rec} is totally kept by the recombined molecule and then the net energy release to the catalyst is:

$$Q_{cat} = Q_{ads}$$

What usually happens is that only part of the energy Q_{rec} is transferred to the surface, and the rest is stored by the desorbing molecule into its vibrational and electronic degrees of freedom. To account for this partial accomodation, the CEA coefficient β has been defined [4]:

$$\beta = \frac{\dot{q}}{\frac{\Delta \dot{n}}{2} D} \tag{1}$$

It is the ratio between the flux of energy actually entering the catalyst surface and the flux of energy entering the surface in case of complete accomodation (in Eq. (1) $\Delta \dot{n}$ is the number of atoms "consumed" by the unit surface in the unit time, so $\frac{\Delta \dot{n}}{2}$ is the flux of recombined molecules). Therefore, for this simple case (i.e., adsorption + ER, assuming ER being a non activated process, $\gamma' = 1$, and steady state), values of β for the two limit situations are:

full accomodation

$$\dot{q} = \frac{\Delta \dot{n}}{2} D \quad \Rightarrow \quad \beta_{max} = 1 \tag{2}$$

no accomodation

$$\dot{q} = \frac{\Delta \dot{n}}{2} Q_{ads} \quad \Rightarrow \quad \beta_{min} = \frac{Q_{ads}}{D} \quad . \tag{3}$$

This latter result is in agreement with the more general one obtained in Ref. [4]:

$$\beta_{min} = \frac{Q_{ads}(1-\theta)}{\gamma' D/2} \tag{4}$$

where, in the assumptions reported above, $\gamma' = 1 - (1-\gamma^*)\theta$ is assumed equal one and, as a consequence, it is $\theta = 0.5$.

A similar simple approach can be followed to show what happens for the LH case. The minimum value of β can be obtained starting from the potential energy curves reported in Fig. 1: we see adsorption of two atoms delivers to the catalyst energy $2 \cdot Q_{ads}$, and the molecule formation via:

$$A^* + A^* \rightarrow A_2 + 2*$$

which is an endothermic process, costs:

$$Q_{rec} = -Q_{LH}$$

Consequently, the overall balance yields (see Fig. 1):

$$Q_{cat} = 2Q_{ads} - Q_{LH} = D \quad .$$

Therefore, by assuming adsorption, LH recombinations activated with energy Q_{LH}, $\gamma' = 1$, and steady state, we have:

$$\beta_{min} = \frac{\frac{\Delta \dot{n}}{2} D}{\frac{\Delta \dot{n}}{2} D} = 1 \quad . \tag{5}$$

Discussion on CEA Process

Experimental findings of recombined molecules desorbing in an vibrational and/or electronic excited state have been reported by Melin and Madix, and Halpern and Rosner that measured β for catalytic recombination of N and O [3] and N [4] for several metal surfaces. The work of Halpern and Rosner is particularly interesting since they have obtained results in a wide range of temperature. The $\beta(T_w)$ trends demonstrate the complexity of the accomodation phenomena. In fact, the simple model set up by Halpern and Rosner assumes that, for metals, heterogeneous recombination of N is dominated at low temperatures by ER (low adatom mobility and high surface coverage) and at high T by LH mechanism (high adatom mobility and low surface coverage). Furthermore these authors assume that ER forms excited molecules which desorb very fast (a gas/surface collision lasts for about a picosecond [15, 16]) so that molecules have very short time to exchange the excess of energy with the surface. Therefore the ER mechanism is predicted to give very low CEA ($\beta < 1$). The LH mechanism, instead, leads to an almost complete accomodation i.e., $\beta \sim 1$. Therefore the expected trend for β predicts low values at low temperatures, increasing with temperature up to a maximum near 1 at the maximum allowable surface temperature. The W surface studied in [4] indeed behaved this way but other materials, e.g., Pt and Ir, presented a maximum before the upper temperature limit, and then values of β decreasing with temperature. Reasons for the failure of the simple model were investigated in the mechanism of chemical energy deposition, and a possible reason for the decrease of β at high temperature (when LH is assumed to be fully activated), was postulated in terms of an incomplete delivery of chemisorption energy of impinging atoms that participate to the LH mechanism. That is, at high temperature, adsorbing N atoms could dissipate their energy very slowly and, before their complete accomodation, could form excited molecules via LH mechanism [4, 17].

This trend of β can also suggest the presence of a third recombination mechanism, the so called *precursor* (PR), in which only one atom is chemisorbed and the other is in a *precursor* state, i.e., an atom which collides with the surface, does not chemisorb, and moves rebounding on it [15]. In this case the precursor atom can keep the major part of its energy yielding a recombination before complete accomodation.

For TPS surfaces a certain number of calorimetric arc-jet measurements of γ exist [9, 18, 19] and comparison with measurements of the atomic recombination coefficients γ' (see Ref. [6] and Ref. 5 cited in [5]) show also very low CEA ($\beta = 0.1 \div 0.2$).

A recent work of Cacciatore et al. [20], based on a semi-classical trajectory approach, studied recombination of O atoms and consequent energy transfer on a SiO_2 surface [1]. Among the interesting conclusions of these authors it is reported the very low energy transfer of ER recombined molecules, which have been found to desorb in a roto-vibrational excited state. Cacciatore et al. suggest that ER recombination occurs in the gas phase just above the surface (at distance > 3.5 Å) and that the energy release to the catalyst surface comes mainly from adsorption of impinging atoms. In this hypothesis, it is $\beta \simeq \beta_{min}$ (e.g., taking $Q_{ads,N} = 330.5$ kJ/mole and $D_{N_2} = 941.8$ kJ/mole [11], and assuming just ER recombinations with $\gamma' = 1$ it is $\beta_{min} = 0.359$; assuming a more realistic $\gamma' = 0.015$ and $\theta = 0.995$ yields $\beta_{min} = 0.224$).

Furthermore, these authors, in contrast with what is reported by Halpern and Rosner for metals, preliminarily conclude that, over a SiO_2 surface at high temperature, the mobility of oxygen atoms is efficiently dumped because of the easy excitation of phonons modes via V-T energy exchange. This leads to a lower probability for LH recombinations as temperature raises (they found the LH probability at 1000 K to be reduced by 0.5 with respect to that at 600 K), and consequently to conclude that the dominant mechanism switches from ER to LH when T decreases. This conclusion has been drawn assuming the same surface coverage at both temperatures and each of those mechanisms acting alone. These could be very strong assumptions. In fact the dominant mechanism is strongly linked to the surface coverage which depends on temperature: ER is much more effective for high surface coverage (low surface coverage means low probability of gas atom-adatom collision) whereas LH has been found efficient for various coverage conditions. Furthermore, control by either ER or LH mechanism influences the surface coverage too, because LH is much more effective in removing atoms then ER; by assuming a surface coverage independent of T means to neglect this interaction. Looking to other authors that have modeled recombination of O over SiO_2, one can see that [10] and [11] assume only ER to be effective from room temperature up to the SiO_2 melting point, whereas [14] and [12] assume LH dominating at high and ER at low temperatures. In any case, At this point, it is difficult to draw general conclusions, but on the basis of the above discussion, we can say that for TPS coating materials the low values of β at high temperature found in the literature could indicate that the ER mechanism could play an important role there or, and this is interesting idea to explore, a PR mechanism could be present.

Chemical Energy Accomodation Modeling

From the above discussion it comes out as incomplete CEA has to be accounted for when, dealing with hypersonic flows simulations, heat loads, and especially fluxes due to heterogeneous catalysis, are under investigation. In this work a simple way to model CEA in CFD simulations of hypersonic flows has been tested: the energy exchange between gas and catalyst has been modified to account for the transfer of chemical energy to vibrational-electronic degrees of freedom of recombined molecules when $\beta \neq 1$. This has been done in the frame of a two

[1] SiO_2 is the substance more widely used to model the borosilicate surface of TPS [13, 11, 14], an assumption supported by experimental results [6].

temperature model where T is the temperature for translational and rotational degrees of freedom and T_V is the temperature for vibrational and electronic degrees of freedom [21].

The energy flux entering the body surface has been written as [8]:

$$\dot{q}_w = \left(k_{tr}\frac{\partial T}{\partial n}\right)_w + \left(k_V\frac{\partial T_V}{\partial n}\right)_w + \left(\rho\sum_{s=1}^{NS}\mathcal{D}_s h_s \frac{\partial X_s}{\partial n}\right)_w + (\dot{q}_R - \epsilon\sigma T_w^4) \quad (6)$$

where NS is the number of chemical species. In this expression we have splitted translational, vibrational, diffusive, and radiative contributions. In our calculations the radiative contribution has not been accounted for.

The diffusive contribution, in the frame of a two temperature model, can been written as:

$$\rho\sum_{s=1}^{NS}\mathcal{D}_s h_s\frac{\partial X_s}{\partial n} = \rho\sum_{s=1}^{NS}\mathcal{D}_s(c_{p,s}^t + c_{p,s}^r)(T - T_{ref})\frac{\partial X_s}{\partial n} + \rho\sum_{s=1}^{NS}\mathcal{D}_s h_{V,s}(T_V)\frac{\partial X_s}{\partial n} + \rho\sum_{s=1}^{NS}\mathcal{D}_s h_s^0\frac{\partial X_s}{\partial n} \quad (7)$$

As already seen, incomplete accomodation means that part of the chemical energy is not released to the catalyst and goes in to the vibrational and electronic degrees of freedom of the catalytically formed molecules. Therefore, we assumed that part of the energy due to the latter contribution in the RHS of Eq. (7), which represents the chemical energy flux entering the surface, is kept by the molecules formed catalytically on the surface:

$$\dot{q}'_{w,V} = \rho\sum_{s=1}^{NS}(1-\beta_s)\mathcal{D}_s h_s^0\frac{\partial X_s}{\partial n} \quad . \quad (8)$$

The amount of this energy flux depends on the value of β: it is zero when $\beta = 1$ and increases when β decreases. Thermal non-equilibrium of catalytically formed molecules has been modeled with an *ad hoc* temperature boundary condition which sets T_w equal to an assigned temperature $\overline{T}$ whereas $T_{Vw} = f(\gamma', \beta)$ is calculated from the flux given by Eq. (8). When $\beta = 1$ both temperatures are set equal to $\overline{T}$.

CFD Code Description

The hypersonic flow is simulated numerically using the code `ARGOS`, a 2D-axisymmetric Navier-Stokes equations solver suitable for thermochemical non-equilibrium flows. The governing equations in conservative form are:

$$\frac{\partial \mathbf{W}}{\partial t} + \nabla\cdot(\mathbf{E}+\mathbf{G}) = \mathbf{H} \quad (9)$$

where the conservative variable vector $\mathbf{W}$, the inviscid flux vector $\mathbf{E}$ and the viscous flux vector $\mathbf{G}$ read:

$$\mathbf{W} = [\rho_s\,,\,\rho\mathbf{u}\,,\,\rho e\,,\,\rho e_V]^T \quad (10)$$

$$\mathbf{F} = [\rho_s\mathbf{u}\,,\,\rho\mathbf{u}\mathbf{u} + p\mathbf{I}\,,\,\rho e\mathbf{u}\,,\,\rho e_V\mathbf{u}]^T \quad (11)$$

$$\mathbf{G} = [\rho\mathcal{D}_s\nabla X_s\,,\,-\boldsymbol{\tau}\,,\,\mathbf{q} - \boldsymbol{\tau}\cdot\mathbf{u}\,,\,\mathbf{q}_V]^T \quad (12)$$

where

$$\boldsymbol{\tau} = \mu\left(\nabla\mathbf{u} + \nabla\mathbf{u}^T\right) - \frac{2}{3}\mu\,(\nabla\cdot\mathbf{u})\,\mathbf{I} \quad (13)$$

$$\mathbf{q} = -k_{tr}\nabla T - k_v\nabla T_V - \rho\sum_{s=1}^{NS}\mathcal{D}_s h_s\nabla X_s \quad (14)$$

$$\mathbf{q}_V = -k_v\nabla T_V - \rho\sum_{s=1}^{NS}\mathcal{D}_s e_{Vs}\nabla X_s \quad . \quad (15)$$

Finally the source terms vector is:

$$\mathbf{H} = [\omega_s\,,\,0\,,\,0\,,\,\omega_{Vs}]^T \quad . \quad (16)$$

Transport properties have been calculated from collision integrals following the approach suggested by Ref [22]. Five chemical species are accounted for (N_2, O_2, N, O, NO), and the chemical rates for each elementary step are expressed in an Arrhenius modified formulation

$$k = AT^B e^{(-E_a/RT)} \quad ,$$

and calculated following the 17 reaction scheme proposed by Dunn and Kang [23]. To account for the effects of vibrational excitation on molecules dissociation, the averaged temperature proposed by Park [21] is used:

$$T_d = T^b T_V^{1-b}$$

with $b = 0.5$. Two contributions are included in the vibrational energy source term, ω_{Vs}: the first accounts for the transfer of energy between translational-rotational and vibrational-electronic modes. The relaxation time is then calculated using the Millikan and White formulation [24] corrected according to Park [21] for high temperatures (> 8000

K). The second contribution accounts for the vibrational energy gain/losses due to chemical reactions. A non-preferential dissociation model is assumed.

Heterogeneous catalysis has been modeled with the approach suggested by Ref. [25] which accounts for heterogeneous formation of N_2 and O_2, with recombination coefficients depending on temperature and atoms concentration.

Numerical Scheme

The system of governing equations Eqs. (9) can be synthetically written as

$$\frac{\partial \mathbf{W}}{\partial t} + \nabla \cdot \mathbf{f} = \mathbf{H}\,. \tag{17}$$

where $\mathbf{f} = \mathbf{E} + \mathbf{G}$. The numerical discretization is obtained by a a cell-centered, finite volume method, and the system (17) is integrated over an elemental volume of the computational domain by a central difference scheme. The adaptive dissipation [26] is included; this model uses a blend of second and fourth differences: the former prevent oscillations near the location of shock waves, the latter are important for stability and convergence to steady state.

Let $\mathbf{S}$ be the directed surface area at the interface $j+1/2$ between the adjacent cells j and $j+1$. The numerical flux evaluated at the interface $j+1/2$ is given by

$$\mathbf{F}_{j+1/2} = \frac{1}{2}\left[\mathbf{F}(\mathbf{W}_j) + \mathbf{F}(\mathbf{W}_{j+1})\right] - \mathbf{D}_{j+1/2}\,.$$

where $\mathbf{F} = \mathbf{f}\cdot\mathbf{S}$. The artificial dissipation term $\mathbf{D}$ has the form

$$\mathbf{D}_{j+1/2} = \lambda_{j+1/2}\Big[\varepsilon^{(2)}_{j+1/2}(\mathbf{W}_{j+1} - \mathbf{W}_j) - \varepsilon^{(4)}_{j+1/2}(\mathbf{W}_{j+2} - 3\mathbf{W}_{j+1} + 3\mathbf{W}_j - \mathbf{W}_{j-1})\Big]\,.$$

The variable scaling factor λ is

$$\lambda_{j+1/2} = \frac{1}{2}\left[\lambda_j + \lambda_{j+1}\right]$$

where

$$\lambda = |\mathbf{u}\cdot\mathbf{S}| + c\,|\mathbf{S}|$$

is the spectral radius of the Jacobian matrix $\partial\mathbf{F}/\partial\mathbf{W}$, with c the speed of sound. The coefficients of the second-difference and fourth-difference dissipation terms are respectively

$$\begin{aligned}\varepsilon^{(2)}_{j+1/2} &= \kappa^{(2)} \max\left(\nu_{j-1}, \nu_j, \nu_{j+1}, \nu_{j+2}\right)\,,\\ \varepsilon^{(4)}_{j+1/2} &= \max\left[0, \left(\kappa^{(4)} - \varepsilon^{(2)}_{j+1/2}\right)\right]\end{aligned}$$

where $\kappa^{(2)}$ and $\kappa^{(4)}$ are constants and ν is the shock "sensor" given by[26]

$$\nu_j = \frac{|p_{j+1} - 2p_j + p_{j-1}|}{\frac{1}{2}\left(\mathcal{P}_{AD} + \mathcal{P}_{TVD}\right)}\,,$$

$$\begin{aligned}\mathcal{P}_{AD} &= p_{j+1} + 2p_j + p_{j-1}\,,\\ \mathcal{P}_{TVD} &= |p_{j+1} - 2p_j| + |p_j - p_{j-1}|\,.\end{aligned}$$

In the calculations of the present work, $\kappa^{(2)}$ and $\kappa^{(4)}$ are 0.8 and 0.03 respectively.

The scheme is second order accurate in space on Cartesian grids. The time integration is performed by a five-stage Runge-Kutta scheme with a point-implicit time-discretization of the chemical source term.

Numerical Tests

A parametric study varying β has been done for a hypersonic air flows over two bodies: a 10° ramp and a cylinder of 3.5 cm radius. Free stream conditions, representative of wind tunnel flows, are shown in Table 2. They present strong thermal nonequilibrium and strong dissociation of chemical species. For the ramp free stream conditions are representative of an F4 (ONERA - France) shot whereas for the cylinder they are representative of an HEG (DLR - Germany) shot.

For both bodies a nickel surface has been assumed and several values of wall temperature have been explored.

Ramp Results

The computational mesh used for this test case is 91 $\times$ 51 nodes and is shown in Fig. 2. β has been set equal to 0.2, 0.5, and 1.0 and three different wall temperatures have been explored: 600, 900, 1200 K. Energy fluxes on the body surface for the case at $T_w = 1200$ K are shown in Figs. 3–6. When β decreases, the diffusive heat flux diminish and the content of vibrational-electronic energy on the surface increases as shown by the rise of T_V (see Figs. 3 and 7). The peak of T_V is located in correspondence of the zone of maximum catalytic activity. This increase of T_V reduces the wall gradient for this temperature and consequently the vibrational-electronic energy flux entering the body as shown by Fig. 4. On the contrary, for decreasing β, the translational-rotational energy flux increases (see Fig. 5). This fact is due to the augment of traslational-rotational energy content of the gas flowing near to the surface originated by vibrationally-electronically excited molecules via V-T energy transfer.

In conclusion, when β decreases, the variations of single contributions lead, to an increase of the global energy flux entering the body (see Fig. 6); passing from $\beta = 1$ to $\beta = 0.2$ the peak heating value increases of 3.4%. For the other two test cases, the peak heating value increase is 2.9% at $T_w = 900$ and 1.7% at $T_w = 600$ K.

Cylinder Results

The computational mesh used for the cylinder test case is 90×60 nodes and is shown in Fig. 8. β has been set equal to 0.2, 0.5, 0.8, and 1.0 and three different wall temperatures have been explored: 500, 800, and 1200 K.

Energy fluxes for the case at $T_w = 1200$ K are shown by Figs. 9–12. For decreasing β, trends are similar to those found for the ramp test case: diffusive, and vibrational energy fluxes diminish and the translational-rotational heat flux augments. However, this last contribution is the largest so that the total energy flux entering the body increases substantially when β reduces; for the peak heating, this increase is of 25% when β passes from 1.0 to 0.2. Vibrational temperature on the surface raises up to 1800 K as shown in Fig. 13.

For the test case at $T_w = 500$ trends are the same (see Figs. 14–17) except for the vibrational-electronical energy flux. In fact, Fig. 15 shows that the lowest energy flux corresponds to the case of complete chemical energy accomodation, i.e., $\beta = 1$. This is due to the very low value of the thermal conductivity k_V has for this low wall temperature ($T_{V,w} = 500$ K). For the other values of β, $T_{V,w}$ grows (see Fig. 18) and the v-e energy flux increases with β.

An overall view of peak heating value trends is given in Figs. 19–22. Diffusive heat flux plots, reported in Fig. 19, show the increase of surface catalytic activity with wall temperature, especially for the highest value. Obviously when CEA reduces, diffusive energy fluxes decrease. Similar behaviour is shown by vibrational-electronic energy fluxes displayed in Fig. 20. In this latter figure, it evident the peculiar behaviour of the case at $T_{V,w} = 500$. Translational-rotational energy fluxes raise when chemical energy accomodation reduces. This occurs for all the temperatures explored and it is due to the increase of temperature gradient at the wall. For the total heat fluxes the trend is well established: reduction of chemical accomodation leads to heat load growth.

From the above results we saw how incomplete accomodation produces a gas in thermal nonequilibrium with high translational and vibrational temperatures. These conditions may increase the dissociation frequency leading to an higher number density of atoms in the gas near to the surface To measure this effect we have used the degree of dissociation $\alpha = N_a/N_A$ where N_a is the number of dissociated atoms and N_A is the total number of atoms present in the gas. Figure 23 reports plots of this quantity evaluated at the first grid point far from the surface in correspondence of the peak heating location. As expected, when chemical accomodation reduces, the gas near to the surface is more dissociated. Furthermore, from this same figure, we see also the change of catalytic recombination effectiveness: in fact passing from $T_w = 500$ K to $T_w = 1200$ K, the dissociation degree reduces because recombination probability γ' increases as shown in Fig. 24 taken from Ref. [25]. Therefore at high T_w the dissociation probability rise is balanced by the increase of catalytic activity. Moreover, for a certain T_w, a rise of atomic species concentration yields a growth of catalytic productions rates.

Conclusions

Chemical Energy Accomodation plays an important role in energy deposition on surfaces interested by heterogeneous catalysis. Experimental results taken from literature report that CEA coefficient β has been found smaller than one for atoms recombinations on both metal and TPS coating surfaces. Mechanisms of energy deposition are still unclear but the low values of β found at high temperatures could lead to conclude that ER recombination mechanism can play an important role and/or a *precursor* recombination mechanism can become important at this conditions of high temperature and low surface coverage.

For the two test cases explored in this study, the CFD simulations show that the effects of varying the chemical accomodation coefficient β are strong on the wall heat flux, which increases when the CEA coefficient β decreases. As diffusive and vibrational-electronic energy fluxes decreases with CEA, this last result is mostly due to the increase of translational-rotational energy flux which was, instead, expected to be of lower intensity.

Effects on the gas phase chemistry are less relevant, and an increase of the degree of dissociation for the gas flowing over the body has been observed. This is due to the decrease of recombination processes in the boundary layer due to the higher translational-rotational temperatures and to the dissociation of vibrationally-electronically excited molecules. This phenomena is smaller for the high wall temperatures where catalytic efficiency raises. The higher concentration of atomic species near to the surface may slightly enhance catalytic recombination.

In conclusion, the boundary conditions implemented to take into account incomplete CEA give results which agree with the expected reduction of diffusive and vibrational-electronic heat fluxes. They are easy to implement and do not imply any extra computational effort. These boundary conditions are suitable for codes using a two temperature model. Their drawback is that is not possible to select which molecular species are excited and how much they are excited.

Acknowledgements

The results contained in this work have been obtained in the frame of the INTAS/RFBR project No. 95-1329. This work has been financially supported by the Sardinian Regional Government. People of the Computer and Network Services Group at CRS4 are gratefully acknowledged.

References

[1] Willey, R.J. "Comparison of Kinetic Models for Atom Recombination on High-Temperature Reusable Surface Insulation". *J. of Thermoph. and Heat Trans.*, 7(1):55–62, Jan-March 1993.

[2] Barbato, M. and Bruno, C. "Heterogeneous Catalysis: Theory, Models and Applications". In M. Capitelli, editor, *Molecular Physics and Hypersonic Flows*, volume C-482 of *NATO-ASI*, pages 139–160. Kluwer Publishers, 1996.

[3] Melin, G.A., Madix, R.J. "Energy Accomodation During Oxygen Atom Recombination on Metal Surfaces". *Chem. Soc. Far. Trans.*, 67(1):198–211, 1971.

[4] Halpern, B. and Rosner, D.E. "Chemical Energy Accomodation at Catalyst Surfaces". *Chem. Soc., Far. Trans. I*, 74:1833–1912, 1978.

[5] Scott, C.D. "Recombination of Atomic Species on Surfaces". In M. Capitelli, editor, *Molecular Physics and Hypersonic Flows*, volume C-482 of *NATO-ASI*, pages 161–180. Kluwer Publishers, 1996.

[6] Carleton, K.L. and Marinelli, W. J. "Spacecraft Thermal Energy Accomodation from Atomic Recombination". *J. of Thermoph. and Heat Trans.*, 6(4):650–655, 1992.

[7] Rosner, D.E. and Feng, H.H. "Energy Transfer Effects of Excited Molecule Production by Surface-catalyzed Atom Recombination". *Chem. Soc., Far. Trans. I*, 70:884–906, 1974.

[8] Bruno, C. "Modeling Catalytic Recombination Heating at High Speed". *AIAA Paper 89-0309*, 1989.

[9] Scott C.D. "Catalytic Recombination of Nitrogen and Oxygen on HRSI". In Crosbie A.L., editor, *Aerothermodynamics and Planetary Entry*, volume 77 of *Progress in Astr. and Aeron.*, pages 193–212. AIAA, 1980.

[10] Seward, W.A. and Jumper, E.J. "Model for Oxygen Recombination on Silicon-Dioxide Surfaces". *J. of Thermoph. and Heat Trans.*, 5(3):284–291, July-Sept. 1991.

[11] Nasuti, F., Barbato, M. and Bruno, C. "Material-Dependent Catalytic Recombination Modeling for Hypersonic Flows". *J. of Thermoph. and Heat Trans.*, 10(1):131–136, Jan.-March 1996.

[12] Deutschmann O., Riedel U., and Warnatz J. "Modeling of Nitrogen and Oxygen Recombination on Partial Catalytic Surface". *ASME J. of Heat Transfer*, 117(2):495–501, 1995.

[13] Suslov, O.N. and Tirskij, G.A. The kinetics of the Recombination of Nitrogen Atoms on HRSI in Hypersonic Thermochemical Non-Equilibrium Flows. In J.J. Hunt, editor, *2nd Europ. Symp. on Aerothermodynamics for Space Vehicles*, pages 413–419. ESA-ESTEC Noordwijk, The Netherlands, 1994.

[14] Daiß, A., Frühauf, H.H., Messerschmid, E.W. "Chemical Reactions and Thermal Nonequilibrium on Silica Surface". In M. Capitelli, editor, *Molecular Physics and Hypersonic Flows*, volume C-482 of *NATO-ASI*, pages 203–218. Kluwer Publishers, 1996.

[15] Masel, R.I. *Principles of Adsorption and Reaction on Solid Surfaces.* John Wiley & Sons, Inc., NY, 1996.

[16] Tully J. "Dynamics of Gas-surface Interactions: Reaction of Atomic Oxygen with Adsorbed Carbon on Platinum". *J. Chem. Phys.*, 73:6333–6342, 1980.

[17] Halpern, B. and Rosner, D.E. "Incomplete Energy Accomodation in Surface-Catalyzed Reactions". In *Heterog. Atmosph. Chem.*, volume 26 of *Geoph. Mon. Series*, pages 167–171. Amer. Geoph. Union, 1982.

[18] Kolodziej P., Stewart D.A. "Nitrogen Recombination on HRSI and the Analysis of its Effects on Surface Catalysis". *AIAA Paper 87-1637, 22nd Thermoph. Conf.*, June 8-10 1987, Honolulu, Hawaii.

[19] Stewart, D.A., Chen, Y.K., Bamford, D.J., Romanovsky, A.B. "Predicting Material Surface Catalytic Efficiency Using Arc-Jet Tests". *AIAA Paper 95-2013, 30th Thermoph. Conf.*, June 19-22 1995, S. Diego, CA.

[20] Cacciatore, M., Rutigliano, M., Billing, G. "Eley-Rideal and Langmuir-Hinshelwood Oxygen Atom Recombination Reaction on Silica: Energy Transfer and Recombination Coefficient Calculation". In *1st Electronic Conference on Vibrational Kinetics in Nonequilibrium Flows*, May 1997. Bari, Italy.

[21] Park, C. *Non-Equilibrium Aerothermodynamics*. John Wiley & Sons, 1990.

[22] Gupta, R.N., Yos, J.M., Thompson, R.A. and Lee, K. "A Review of Reaction Rates and Thermodynamic and Transport Properties for an 11-Species Air Model for Chemical and Thermal Nonequilibrium Calculations to 30,000 K". Technical Report RP 1232, NASA, 1990.

[23] Dunn, M.C. and Kang, S.W. "Theoretical and Experimental Studies of Re-entry Plasmas". Technical Report CR-2232, NASA, 1973.

[24] Millikan, R.C. and White, D.R. "Systematics of Vibrational Relaxation". *Chemical Physics*, 39, 1963.

[25] Reggiani, S., Barbato, M., Bruno, C., and Muylaert, J. "Model for Heterogeneous Catalysis on Metal Surfaces with Applications to Hypersonic Flows". *AIAA Paper 96-1902, 31st AIAA Thermophysics Conference*, June 17-20 1996, New Orleans, LA.

[26] Swanson, R. C. and Turkel, E. "On central-difference and upwind schemes". *J. Comput. Phys.*, 101, 1992.

Table 1: Heterogeneous kinetics elementary steps. Steps I-IV and VI are included in the catalysis model used in this work (see Ref. [25])

.

$A^G + * \rightarrow A*$	chemisorption of atoms	I
$A_2^G + 2* \rightarrow A * + A*$	chemisorption of molecules	II
$A^G + A* \rightarrow A_2^G + *$	Eley-Rideal recombination	III
$A* + A* \rightarrow A_2^G + 2*$	Langmuir-Hinshelwood rec.	IV
$A^P + A* \rightarrow A_2^G + *$	Precursor rec. mechanism	V
$A* \rightarrow A^G + *$	thermal desorption	VI

Table 2: Free stream conditions for the CFD simulations.

	F4	HEG
U_∞ (m/s)	5616.5	4211.35
ρ_∞ (kg/m^3)	0.00690	0.02244
L (m)	0.38	0.035
T_∞ (K)	299.8	1106.34
$T_{V\infty}$ (K)	5655.0	2225.66
Ma	12.8	6.2
Y_{N_2}	0.7732	0.7406
Y_N	0.0019	0.000
Y_{O_2}	0.0039	0.1646
Y_O	0.2151	0.0377
Y_{NO}	0.0059	0.0571

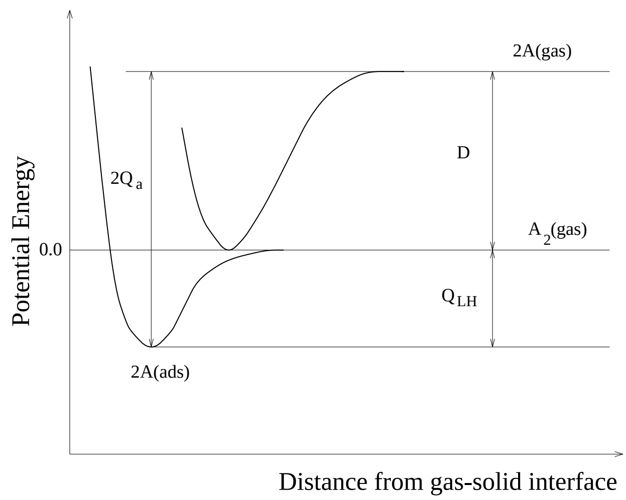

Figure 1: Potential energy diagram for a generic LH recombination. Figure adapted from Ref. [4].

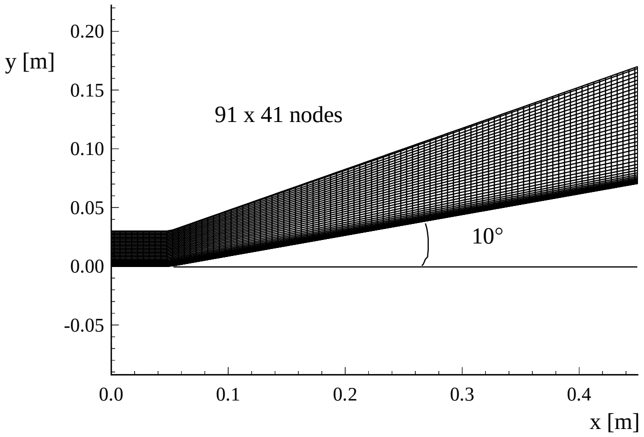

Figure 2: Ramp in F4 – computational mesh.

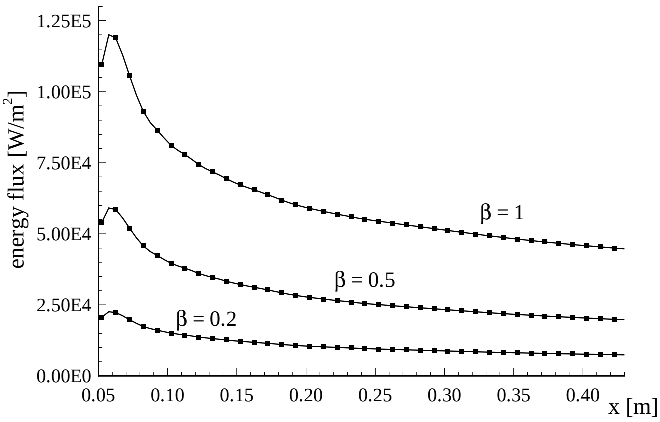

Figure 3: Ramp in F4 – comparison of diffusive energy fluxes varying β (T_w = 1200 K).

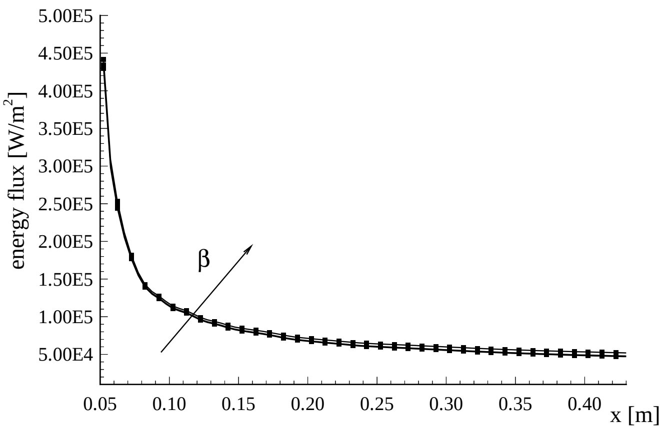

Figure 4: Ramp in F4 – comparison of vibrational-electronic energy fluxes varying β (T_w = 1200 K).

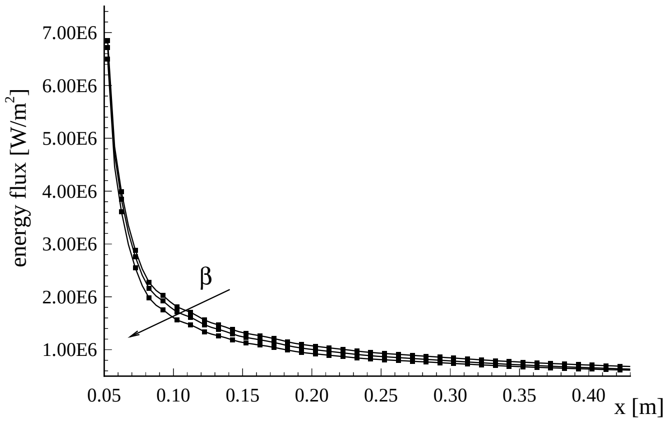

Figure 5: Ramp in F4 – comparison of translational-rotational energy fluxes varying β (T_w = 1200 K).

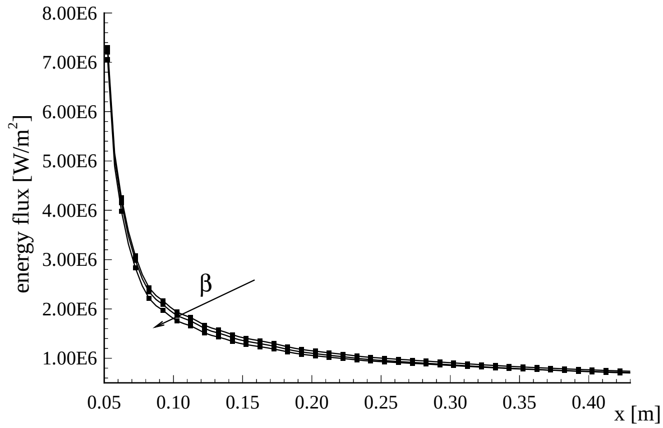

Figure 6: Ramp in F4 – comparison of total energy fluxes varying β (T_w = 1200 K).

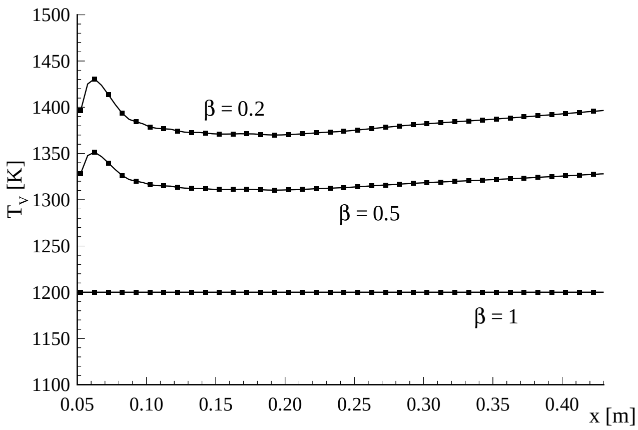

Figure 7: Ramp in F4 – vibrational-electronic temperature on the body surface obtained varying β (T_w = 1200 K).

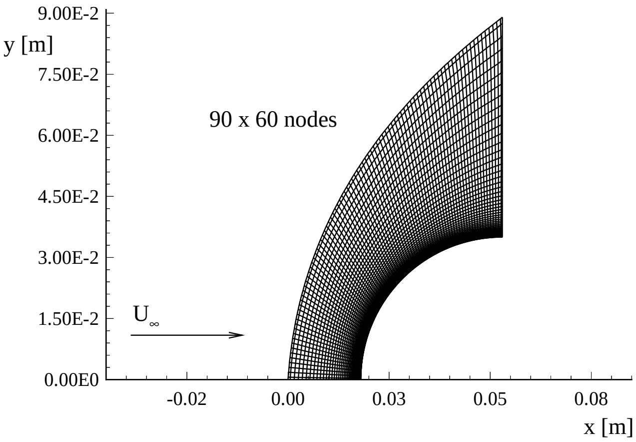

Figure 8: Cylinder in HEG – computational mesh.

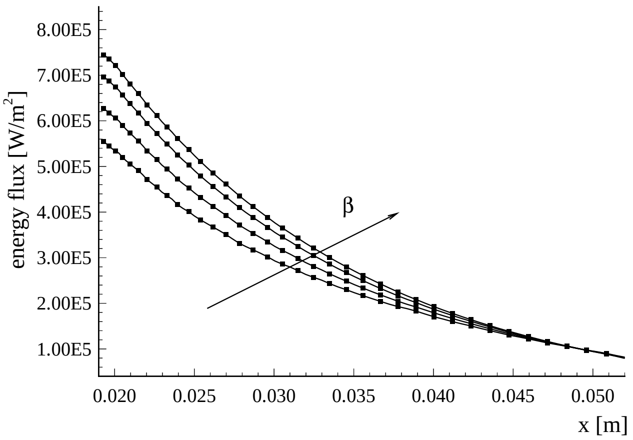

Figure 10: Cylinder in HEG. Comparison of vibrational-electronic energy fluxes varying β (T_w = 1200 K).

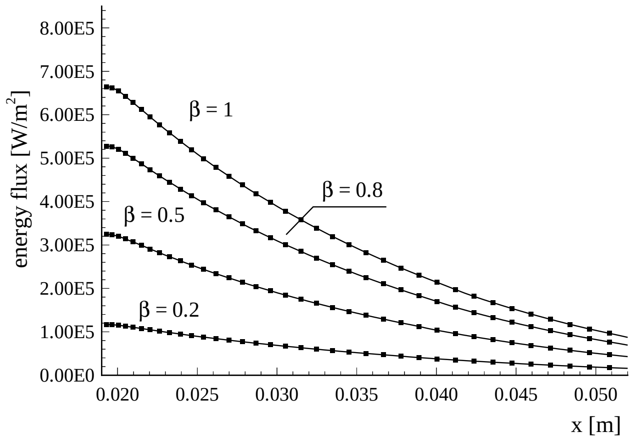

Figure 9: Cylinder in HEG. Comparison of diffusive energy fluxes varying β (T_w = 1200 K).

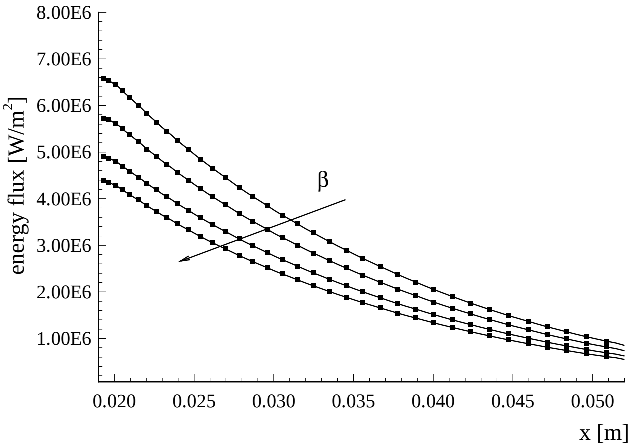

Figure 11: Cylinder in HEG. Comparison of translational-rotational energy fluxes varying β (T_w = 1200 K).

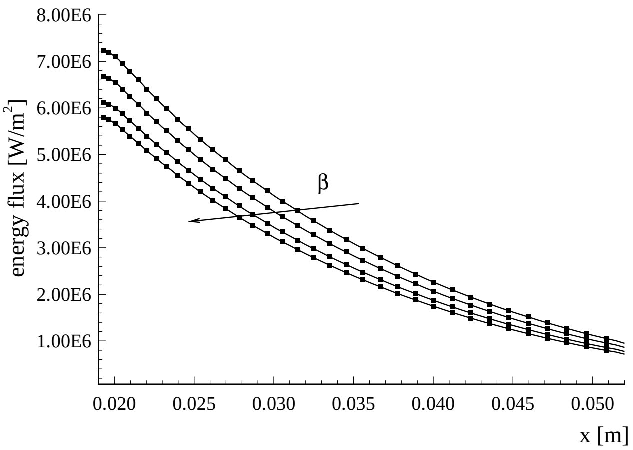

Figure 12: Cylinder in HEG. Comparison of total energy fluxes varying β (T_w = 1200 K).

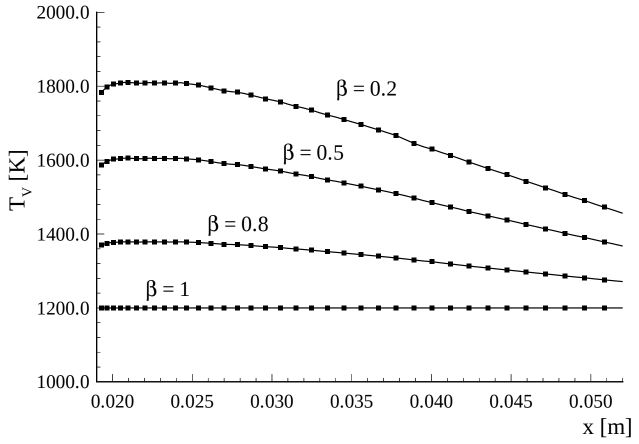

Figure 13: Cylinder in HEG. Vibrational-electronic temperature on the body surface obtained varying β ($T_w = 1200$ K).

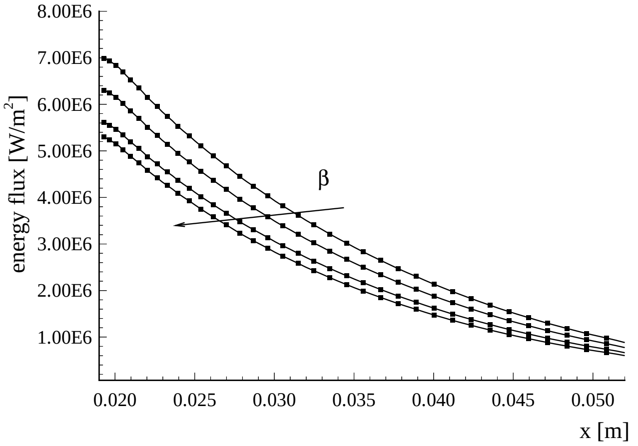

Figure 16: Cylinder in HEG. Comparison of translational-rotational energy fluxes varying β ($T_w = 500$ K).

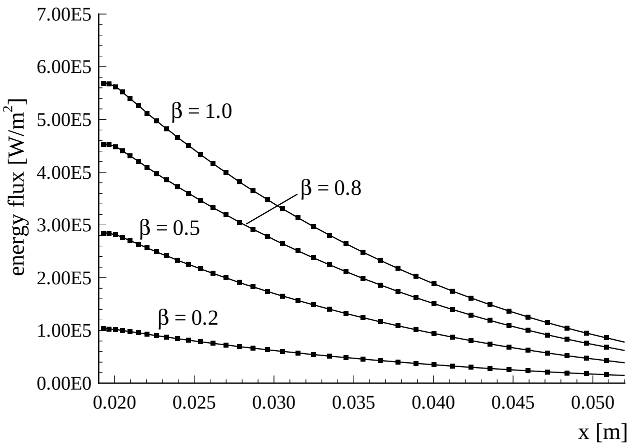

Figure 14: Cylinder in HEG. Comparison of diffusive energy fluxes varying β ($T_w = 500$ K).

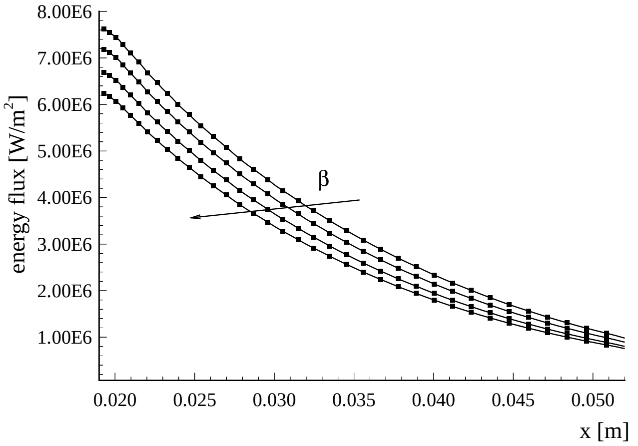

Figure 17: Cylinder in HEG. Comparison of total energy fluxes varying β ($T_w = 500$ K).

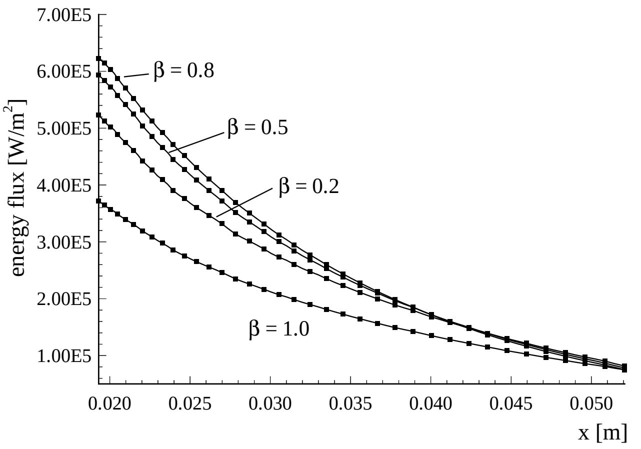

Figure 15: Cylinder in HEG. Comparison of vibrational-electronic energy fluxes varying β ($T_w = 500$ K).

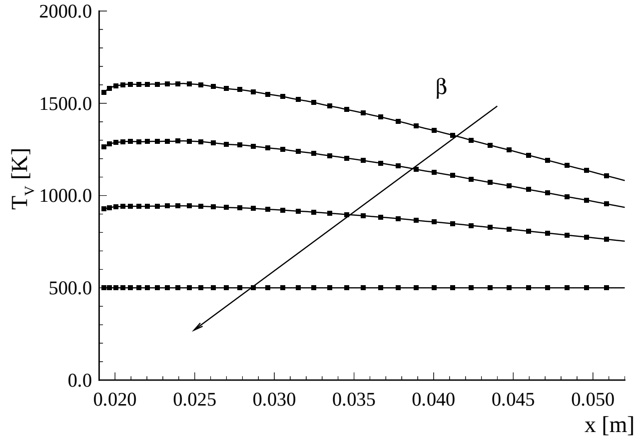

Figure 18: Cylinder in HEG. Vibrational-electronic temperature on the body surface obtained varying β ($T_w = 500$ K).

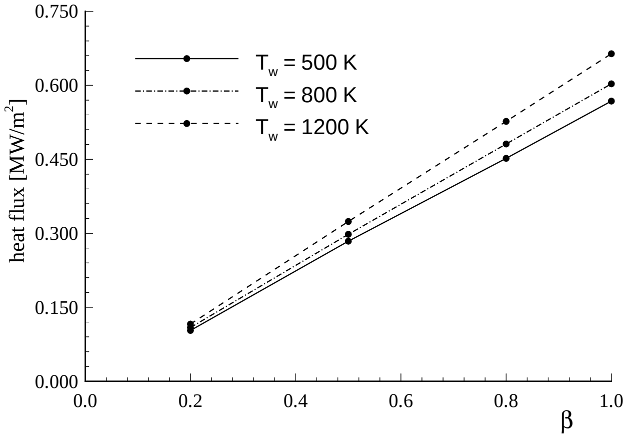

Figure 19: Cylinder in HEG. Peak value for diffusive energy flux: comparison varying β and body temperature.

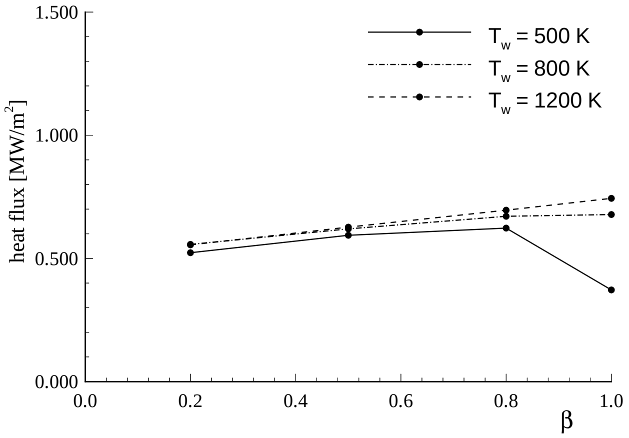

Figure 20: Cylinder in HEG. Peak value for vibrational-electronic energy flux: comparison varying β and body temperature.

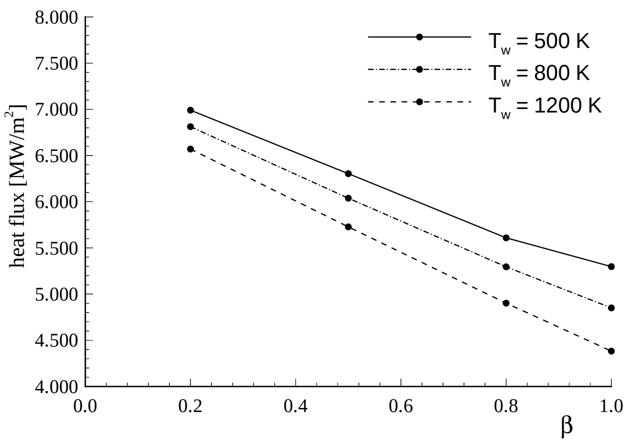

Figure 21: Cylinder in HEG. Peak value for translational-rotational energy flux: comparison varying β and body temperature.

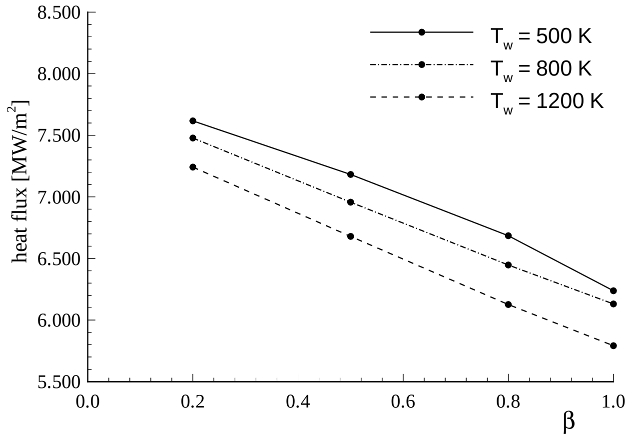

Figure 22: Cylinder in HEG. Peak value for the total energy flux: comparison varying β and body temperature.

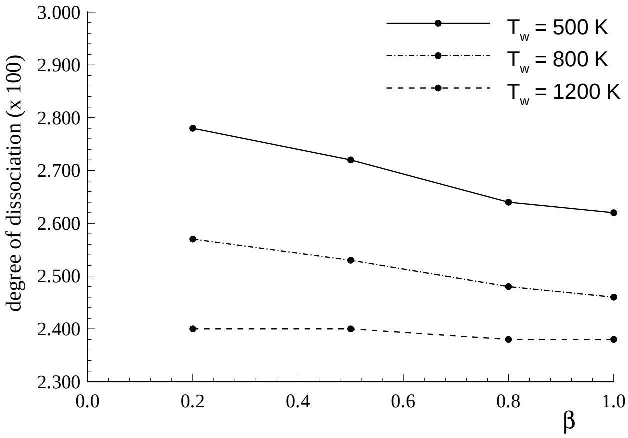

Figure 23: Cylinder in HEG. Dissociation degree calculated at the first grid point far from the surface in correspondence of the peak heating location.

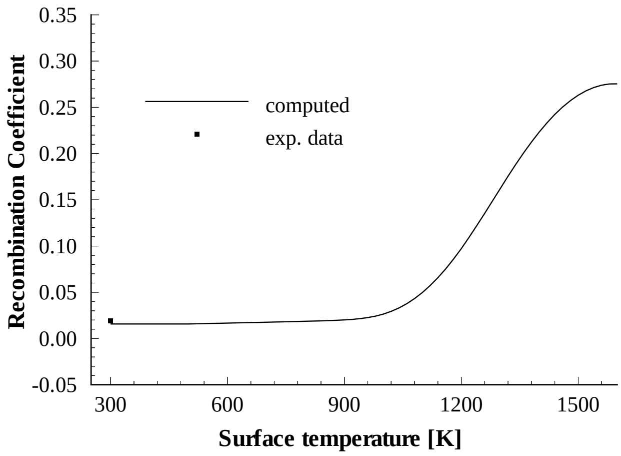

Figure 24: Oxygen recombination on Ni: comparison between model results and experimental data. From Ref. [25].